Geomorphology 303 (2018) 162–171

Contents lists available at ScienceDirect

Geomorphology

journal homepage: www.elsevier.com/locate/geomorph

Connection of the proto-Yangtze River to the East China Sea traced by sediment magnetic properties

Xianbin Liu [a], Jing Chen [a,*], Barbara A. Maher [b], Baocheng Zhao [c], Wei Yue [a], Qianli Sun [a], Zhongyuan Chen [a]

[a] State Key Laboratory of Estuarine and Coastal Research, East China Normal University, Shanghai 200062, China
[b] Centre for Environmental Magnetism & Palaeomagnetism, Lancaster Environment Centre, University of Lancaster, LA1 4YQ, UK
[c] Shanghai Institute of Geological Survey, Shanghai 200072, China

ARTICLE INFO

Article history:
Received 23 November 2016
Received in revised form 27 November 2017
Accepted 27 November 2017
Available online 5 December 2017

Keywords:
Yangtze River
Plio-Quaternary stratigraphy
Sediment magnetic properties
Magnetic susceptibility
Sediment source-sink
Cenozoic topographic reversal

ABSTRACT

The evolution of the Yangtze River, and specifically how and when it connected to the East China Sea, has been hotly debated with regard to possible linkages with the so-called 'Cenozoic Topographic Reversal' (tectonic tilting of continental east China in the Cenozoic) and particularly the relationship to the uplift history of the Tibetan Plateau. Resolving this key question would shed light on the development of large Asian rivers and related changes in landforms and monsoon climate during this interval. Here, we use the magnetic properties of both Plio-Quaternary sediments in the Yangtze delta and of surficial river sediments to identify a key mid-late Quaternary switch in sediment source-sink relationships. Our results reveal a fundamental shift in sediment magnetic properties at this time; the upper 145 m of sediment has magnetic mineral concentrations 5 to 10 times higher than those of the underlying late Pliocene/early Quaternary sediments. We show that the distinctive magnetic properties of the upper core sediments closely match those of surficial river sediments of the upper Yangtze basin, where the large-scale E'mei Basalt block (2.5×10^5 km^2) is the dominant magnetic mineral source. This switch in sediment magnetic properties occurred at around the Jaramillo event (~1.2–1.0 Ma), which indicates that both the westward extension of the proto-Yangtze River into the upper basin and completion of the connection to the East China Sea occurred no later than at that age.

1. Introduction

The evolution of large (continental-scale) rivers has been the focus of much international research in past decades in relation to tectonic, climatic, and base-level changes (Said, 1981; Hoorn, 1994; Clark et al., 2004). In particular, the development of large Asian rivers has attracted much attention, reflecting their associations with Cenozoic Tibetan Plateau uplift, which has had a key influence on both Asian landforms and monsoon climate during this period (Fig. 1A; Brookfield, 1998; Clark et al., 2004; Wang et al., 2005; Clift et al., 2006).

Early studies of the Yangtze River discussed its formation in relation to the complicated tectono-geomorphological processes that affected the Chinese continental craton. Those studies hypothesized that the river previously (age undetermined) drained southward into the South China Sea along the present course of the Red River (Song Hong) in the upper Yangtze basin (Fig. 1A; Wang, 1985a, 1985b; Brookfield, 1998). Subsequently, the proto-Yangtze river was captured at Shigu (Fig. 1B), the first-bend of the upper basin ~150 km above the Red River's headwaters. It was suggested that proto-Yangtze capture was driven by disruption of the paleo-drainage and topographic movement in relation to tilting of the southwestern Yangtze craton (Wang, 1985a; Wang, 1985b; Clark et al., 2004). This tectono-geomorphological process, accompanied by immense tectonic subsidence of the mid-lower Yangtze basin, is thought to have eventually induced the river to flow eastward into the East China Sea, traversing a distance of ~6300 km (Fig. 1A, B).

The Three Gorges Valley of the upper Yangtze River, another key geomorphological location, links the upper plateau and the mid-lower Yangtze fluvial plain system (Fig. 1B). The proto-Yangtze could only have become connected to the East China Sea with the opening of the Three Gorges Valley. Dating of a series of terraces in the Three Gorges (by electron spin resonance) indicates that the oldest terrace formed at ~1.16 Ma (Li et al., 2001). Furthermore, basaltic gravels in the mid-Pleistocene alluvial fan deposits of the middle Yangtze basin (i.e. below the Three Gorges Valley) have been attributed to an upper Yangtze basin source (Xiang et al., 2007), which implies an opening of the Three Gorges at ~1.1 Ma. Richardson et al. (2010) suggested that the onset of incision of Three Gorges Valley was linked to orogenic erosion and associated river capture processes in central China, dated at 40–45 Ma. The final date of opening of Three Gorges Valley remains disputed.

In recent years, numerous studies have sought to explore the evolution of eastward connection of the Yangtze River to the sea by using a

* Corresponding author.
E-mail address: jchen@geo.ecnu.edu.cn (J. Chen).

https://doi.org/10.1016/j.geomorph.2017.11.023
0169-555X/

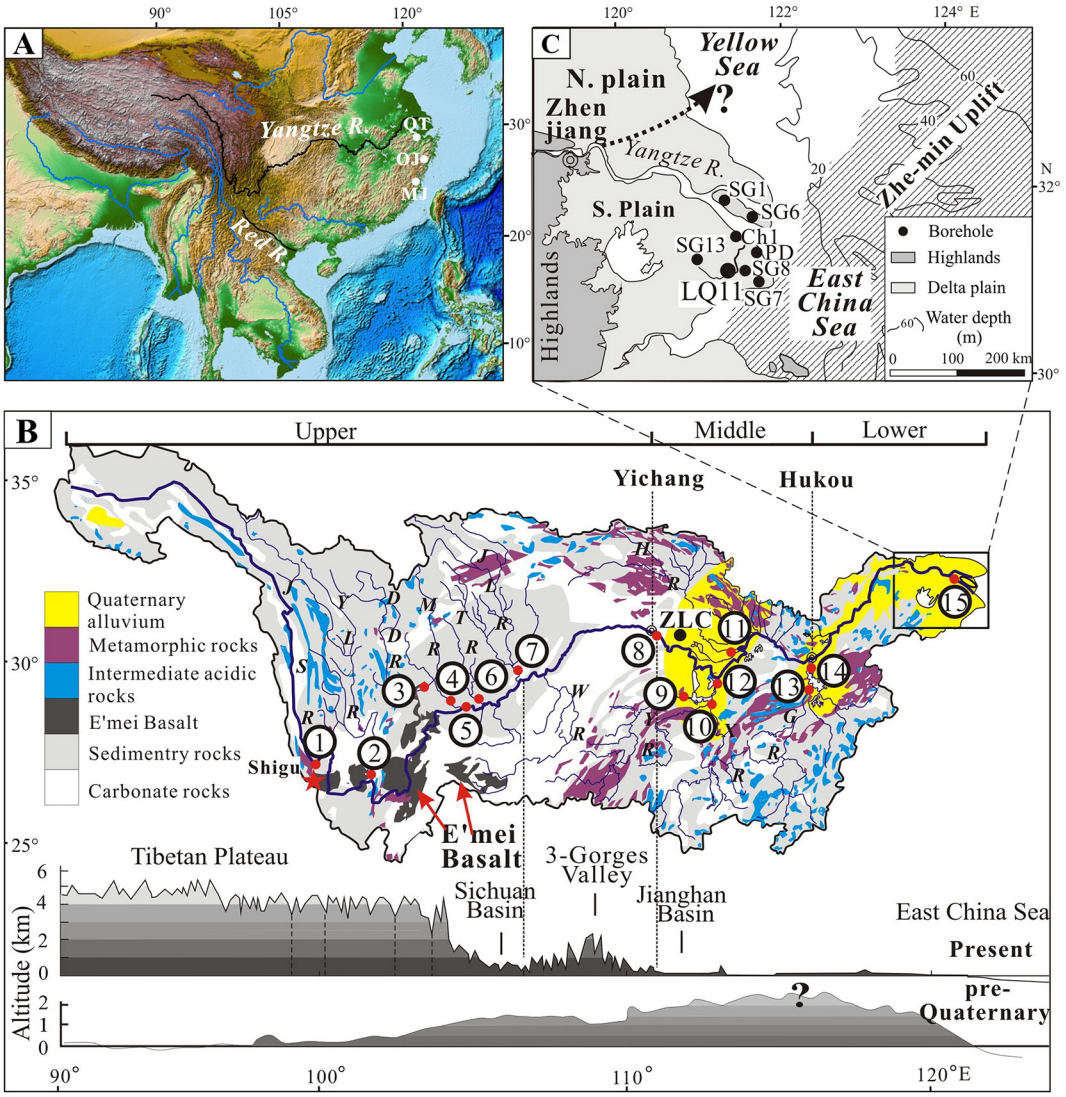

Fig. 1. A) Locations of large Asian rivers in relation to the Tibetan Plateau. B) The Yangtze River basin, with: the large-scale E'mei Basalt block in the upper Yangtze basin (above the Three Gorges Valley) indicated by red arrows; tributaries and sampling sites: ① Shigu; ② Yalong River (YLR); ③ Dadu River (DDR); ④ Min River (MR); ⑤ Jinsha River (JSR); ⑥ Tuo River (TR); ⑦ Jialing River (JLR); ⑧ Three Gorges (Yichang); ⑨ Yuan River (YR); ⑩ Xiang River (XR); ⑪ Han River (HR); ⑫ Dongting Lake (DTL); ⑬ Gan River (GR); ⑭ Poyang Lake (PYL); ⑮ River Mouth; the E'mei Basalt site (star); Zhoulao Core (ZLC), from the middle Yangtze basin, below the Three Gorges Valley (Zhang et al., 2008). The Cenozoic Topographic Reversal of the eastern China continent is modified after Wang (1990). C) Sites of sediment cores on the delta coast. The shaded zone off the Yangtze River mouth represents the Tertiary Zhe-Min uplift. Surficial samples, QT, OJ, and MJ (Fig. 1A) were taken from the exposure of the Zhe-Min uplift along the coast (Cao et al., 2014). The arrow in C indicates another possible route of the proto-Yangtze connection to the sea.

range of sediment provenance proxies on delta sediment cores, especially monazite age patterns and detrital zircon U-Pb ages (Fan et al., 2005; Yang et al., 2006; Zheng et al., 2013; Gu et al., 2014; Yue et al., 2016). Although effective, these proxies demonstrate generic linkages to potential rock sources in the river basin and uncertainties remain (cf. Malusà et al., 2016). Of note, the westward extension of the river and its connection to the sea has been dated variably, ranging from ca. 23 to 1.0 Ma (cf. Gu et al., 2014).

Iron-bearing minerals are sensitive to environmental change in relation to sediment source, transport, and deposition in the absence of substantial authigenesis and post-depositional alteration (Thompson and Oldfield, 1986). Hence, sediment magnetic properties have been used widely in studies of paleoenvironmental change and sediment provenance (Liu et al., 2012). Here, we use this approach to examine the spatiotemporal distribution of magnetic properties of long cores and of surficial Yangtze River sediments to identify diagnostic magnetic properties for use as sediment tracers. We then match sedimentary magnetic signatures to specific sediment sources in the Yangtze River basin. Finally, we determine, by magnetostratigraphy, the timing of eastward connection of the Yangtze River to the sea. Our magnetic approach is complemented by independent, integrated analysis of sedimentary facies and foraminiferal assemblages.

2. Study area

The Yangtze River is ~6300 km long, with an immense drainage basin area of ~1.8×10^6 km^2. The river drains from west to east, emptying into the East China Sea, across the three major topographic steps of the Chinese continent (Fig. 1A, B). The river basin can be divided into the upper, middle and lower reaches on the basis of geomorphologic features.

The upper reach covers an area of ~1.0×10^6 km^2 from its source in the Tibetan Plateau to the end of the Three Gorges Valley at Yichang. Within this upper reach, the elevation ranges between 2000 and 4000 m above mean sea level (Fig. 1A, B). Rock exposures predominantly comprise Paleozoic-Mesozoic carbonate and clastic sedimentary

rocks (Changjiang Water Resources Commission, 1999). A large-scale Mesozoic basaltic outcrop, the E'mei Basalt block (2.5×10^5 km^2), occurs exclusively in the upper basin (Fig. 1B). The main tributaries that join the upper Yangtze mainstream include the Yalong River, Min River, Jialing River, Wu River and Tuo River (Fig. 1B). The middle Yangtze River reach is ~950 km in length, extending from Yichang to Hukou (Fig. 1B).

This middle reach is a typical meandering river system with an extensive floodplain covering an area of 0.68×10^6 km^2 extending from Yichang to Hukou (Fig. 1B). The Han River, Dongting Lake, and Poyang Lake are the three main flows that join the Yangtze mainstream in this area (Fig. 1B). Below Hukou is the lower Yangtze reach, which extends about 930 km to the East China Sea. No major tributaries adjoin this reach, except Taihu Lake in the lower delta plain (Fig. 1B, C). The middle and lower Yangtze basin is dominated primarily by Paleozoic-Mesozoic sedimentary rocks and unconsolidated Quaternary sediments, with some intermediate-acidic igneous rocks and metamorphics (Changjiang River Water Resources Commission, 1999). Finally, the extensive delta system at the Yangtze River mouth covers an area of >25,000 km^2 (Fig. 1C).

3. Data and methods

A continuous sediment core (LQ11), which was 301-m long and penetrated the Plio-Quaternary strata to bedrock, was recovered by rotary drilling from the southern Yangtze delta plain (Fig. 1C). The core was split in the laboratory, one half for sampling and the other for archiving. The sediment core was photographed (Fig. S1) and logged continuously, with descriptions made of lithology, sediment color, bedding stratification, root traces, and bioturbation.

A total of 279 samples was taken for grain size analysis with a sampling interval of ~1.0 m. A laser particle size analyzer (CoulterLQ-100) was used to measure sediment particle sizes from 0.02 to 2000 μm at the State Key Laboratory for Estuarine and Coastal Research (SKLEC), East China Normal University, Shanghai. Samples were pre-treated with H_2O_2 and HCl to remove organic matter and carbonate, respectively. Sodium hexametaphosphate $(NaPO_3)_6$ was added to disaggregate samples via ultrasonic dispersion prior to analysis.

A total of 539 oriented samples was taken for paleomagnetic analysis at sampling intervals of ~30 cm in fine-grained sediment, and ~1.0 m in sandy sediment. No samples were taken in gravelly sands, which often occurred in the mid-lower part of the core. Paleomagnetic analysis followed standard procedures: 1) stepwise thermal demagnetization was done using an ASC TD-48 thermal demagnetizer, from room temperature to 585/680 °C with a measurement interval of 10–50 °C; 2) sediment remanent magnetizations were measured with a 2-G Enterprises cryogenic magnetometer in a magnetically shielded room (<150 nT) at the Institute of Earth Environment, Chinese Academy of Sciences (IEECAS), Xi'an, China. Demagnetization results were evaluated by orthogonal diagrams (Zijderveld, 1967) and the characteristic remanent magnetization (ChRM) was determined by principal component analysis (Kirschvink, 1980).

A total of 277 core samples was taken for sediment magnetic property measurements. Magnetic susceptibility (χ_{lf} and χ_{hf}) was measured using a Bartington Instruments MS2 Susceptibility Meter at low (0.47 kHz) and high (4.7 kHz) frequencies. Anhysteretic remanent magnetization (ARM) was measured using a DTECH 2000 demagnetizer with a peak alternating field (AF) of 100 milliTesla (mT) and direct current (DC) bias field of 0.05 mT. Isothermal remanent magnetizations (IRMs) were imparted using an MMPM10 pulse magnetizer. Samples were first subjected to a DC field of 1 T, to generate a 'saturation' IRM (SIRM), followed by application of a −300 mT backfield. All remanences were measured with a Minispin magnetometer. S_{-300} was calculated as: $S_{-300} = (SIRM - IRM_{-300\ mT})/(2 \times SIRM)$ (Bloemendal et al., 1992).

Representative core samples with large χ_{lf} fluctuations (<15 $\times 10^{-8}$ m^3/kg and >60 $\times 10^{-8}$ m^3/kg) were selected for additional measurements, including 12 samples for IRM acquisition curves and high-temperature magnetization (Ms–T curves) measured at SKLEC; 3 samples for scanning electron microscope (SEM) observation and energy-dispersive spectra (EDS) analysis at Yuyi Analytic, Shanghai, China. IRM acquisition curves were obtained using stepwise increasing fields 50, 100, 200, 300, 500, 800, and 1000 mT. First-order reversal curve (FORC) analysis (Pike et al., 1999) for 8 samples was made using with a Princeton Measurements Corporation vibrating sample magnetometer (VSM 3900) at Baoji University of Arts and Sciences. For each sample, 150 FORCs were measured with fields up to ~300 mT, an averaging time of 200 ms and a smallest field increment of 1.2–1.5 mT. Data were processed using the algorithm of Heslop and Roberts (2012) with a smoothing factor (SF) of 5.

Forty one core samples were tested for total organic carbon (TOC) content using potassium dichromate oxidation-ferrous sulphate titrimetry. Sixty-five surficial river sediment samples were taken from 15 sites located in the mainstream and major tributaries of the Yangtze River (Fig. 1B). One exposed basalt sample was also taken from the E'mei Basalt block (Fig. 1B). Magnetic measurements followed the same procedures as used for core samples.

In addition, 163 samples were taken from sediment core LQ11 for foraminifera identification using a binocular microscope (Wang, 1985a, 1985b; Zheng and Fu, 2000). Seven representative Plio-Quaternary sediment cores with magnetic susceptibility and OSL, ESR, U-series, ^{14}C dating were collected from the Yangtze delta (Figs. 1C, 3; Qiu and Li, 2007; Wang et al., 2008; Chen et al., 2014; Gu et al., 2014). The Plio-Quaternary Zhoulao core was also collected from the middle Yangtze basin and has a detailed rock magnetic property record including χ_{lf}, χ_{ARM}, and SIRM (Fig. 1B; Zhang et al., 2008). Data from these cores provide additional information for the present study.

4. Results

Sediment core LQ11 and other collected cores provide information on the chronostratigraphy, lithology, and sedimentary facies of the study area (Figs. 2, 3). Results are detailed below.

4.1. Chronostratigraphy

In general, demagnetization data for representative samples in core LQ11 have a relatively straightforward unidirectional trajectory toward the origin of demagnetization diagrams from 200 to 300 °C to 585/680 °C (Fig. 4). The demagnetization behavior indicates that magnetite is the main ChRM carrier for most samples, and that hematite is also an important ChRM carrier for some samples (Fig. 4). 326 out of 539 paleomagnetic samples (60%) yield reliable ChRM directions according to two criteria that at least 4 consecutive demagnetization steps must be used to define the ChRM and the maximum angular deviation (MAD) must be <15°.

Paleomagnetic analysis of the LQ11 sediments reveals the (normal polarity) Gauss epoch at a depth between 300 and 252 m and the (reversed polarity) Matuyama epoch between 252 and 112 m; hence, the Pliocene/Pleistocene boundary occurs at 252 m (2.60 Ma) (Fig. 2). The Olduvai and Jaramillo subchrons are recognized at depths of 186–159.9 m and 145.2–120.8 m, respectively. The normal polarity Brunhes epoch is evident above 112 m (Fig. 2).

Although gravelly sands occur frequently in the mid-lower part of sediment core LQ11, which inevitably affects paleomagnetic sampling and data quality, the comparability of our paleomagnetic chronology with other published chronostratigraphic data, including OSL, ESR, U-series, and ^{14}C dating from other cores provides a reliable baseline for Plio-Quaternary division of sediments in the study area (Fig. 3; Qiu and Li, 2007; Wang et al., 2008; Chen et al., 2014).

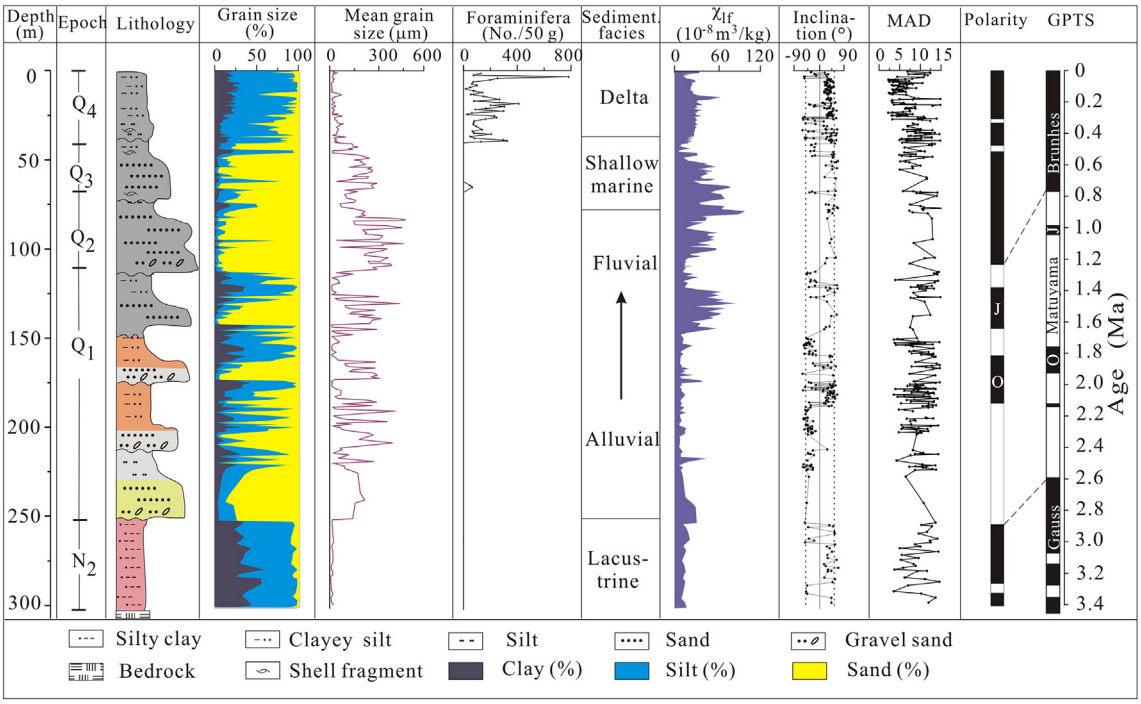

Fig. 2. Magnetostratigraphy, magnetic susceptibility (χ_{lf}), lithology, grain size, foraminifera, and sedimentary facies of core LQ11. The geomagnetic polarity timescale (GPTS) is from Cande and Kent (1995). Only the samples with MAD <15° are shown. N_2: Pliocene; Q_1: Early Pleistocene; Q_2: Middle Pleistocene; Q_3: Late Pleistocene; Q4: Holocene.

4.2. Lithology

A thick, basal, reddish Pliocene mudstone rests unconformably on regional bedrock at a depth of 301–252 m (Figs. 2, S1). The mean grain size of the mudstone ranges from 7 to 24 μm. The Early Pleistocene strata (252–112 m) contain at least 3–4 sedimentary cycles consisting of basal yellowish-grey gravelly sands and coarse sand, topped by greyish brown fine sediments (sand, silt, and clay) (Figs. 2, S1). The mean grain size of the coarse sand units ranges from 450 μm (maximum) to 9.1 μm (minimum). Large-scale cross-stratification was

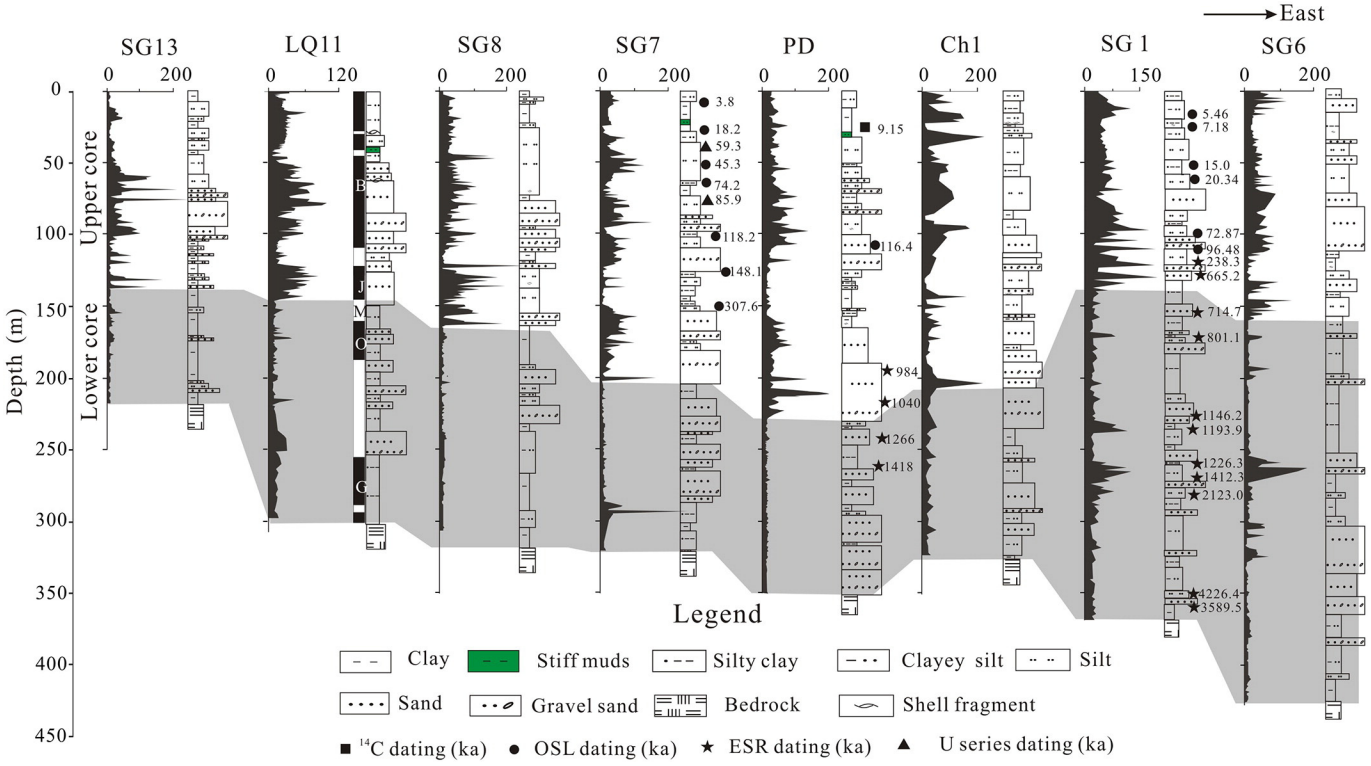

Fig. 3. Magnetic susceptibility profiles for sediment cores from the Yangtze delta. Noted is the high (white background) and low (grey background) magnetic susceptibility in the upper and lower portions of Plio-Quaternary sediments (Age data: core SG1, Qiu and Li, 2007; core SG7, Wang et al., 2008; core PD, Chen et al., 2014; magnetic susceptibility and lithology data: Gu et al., 2014). N_2 and Q_{1-4} are as in Fig. 2.

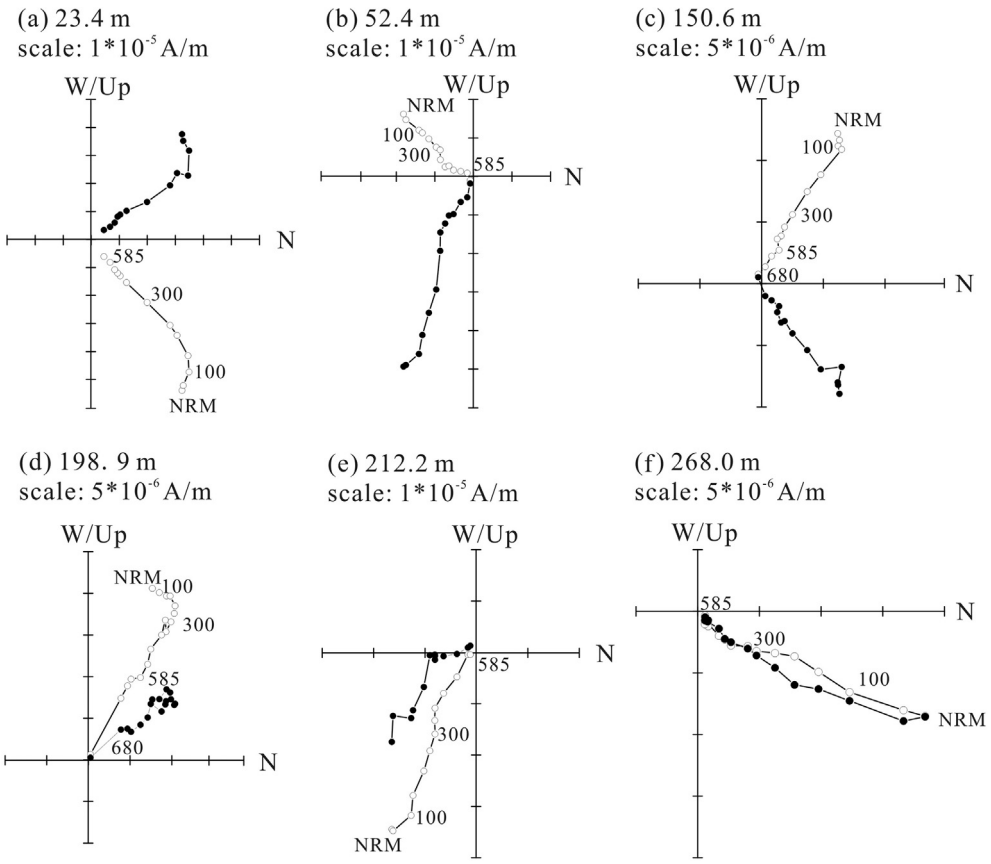

Fig. 4. Orthogonal projections of progressive thermal demagnetization results for representative samples of core LQ11. Open and closed circles indicate projections onto the vertical and horizontal planes, respectively. The numbers indicate temperatures in °C. NRM is natural remanent magnetization.

evident in these sand units. For the Middle Pleistocene sediments (112–67.6 m), yellowish-grey gravelly sands (minor in proportion) alternate with coarse to fine sand units. Cross-stratification is also frequent in these units (Figs. 2, S1). Mean grain size ranges from 480 to 18 μm. The Late Pleistocene strata (67.6–41.3 m) consist of thick, cyclic units, comprising greyish coarse sands, topped by thick, grey fine sand and silt (299.6–18.7 μm mean grain size) (Figs. 2, S1). Wavy and horizontal bedding prevail in this Late Pleistocene material. Fine sand and silty clay, or clayey silt, occur from 41.3 to 0 m in Holocene strata (100.2–9.7 μm mean grain size). A thin layer (42.20–41.30 m) of stiff muds separates the Holocene sediment from the underlying Late Pleistocene material (Figs. 2, S1). Shell fragments (often of brackish origin, e.g. *Tellina jedoensis*, *Gulalius*, *Retusa*, etc.; Qiu and Li, 2007) occur in the late Pleistocene-Holocene strata. Sand-mud couplets, formed as horizontal bedding in tidal flat facies, are common in the Late Quaternary strata (Fig. S1).

4.3. Magnetic properties of sediment core LQ11

Temporal variations of magnetic susceptibility (χ_{lf}), together with other magnetic properties, divide the Plio-Quaternary sediments of core LQ11 into two major portions (Fig. 5A). Low and relatively unvarying χ_{lf} values (mostly $<15 \times 10^{-8}$ m^3/kg) occur in the lower part of the core (301–145 m). This low magnetic mineral content is associated with low SIRM and S_{-300} and high χ_{ARM}/χ_{lf}, and χ_{ARM}/SIRM values. In marked contrast, high χ_{lf} values occur as 3 large-amplitude intervals in the upper portion of the core (145–0 m) (Fig. 5A). These high χ_{lf} values are accompanied by high SIRM and S_{-300} and low χ_{ARM}/χ_{lf} and χ_{ARM}/SIRM values (Fig. 5A).

The magnetic mineralogy throughout core LQ11 is dominated by magnetite, as indicated by Ms.–T curves with a major decrease near 580 °C for most representative samples (Fig. 6a–d). The magnetite has characteristic pseudo-single domain (PSD)/multi-domain (MD) behavior (Roberts et al., 2000, 2014), revealed by FORC diagrams with more divergent contours along the Hu axis (>60 mT) and a low coercivity distribution along the Hc axis (<80 mT) (Fig. 6e–h). A lesser contribution from hematite is evidenced by a slight magnetization decrease up to 680 °C (Fig. 6a–d). SEM observations and O and Fe peaks in EDS results also indicate that the magnetic minerals consist mainly of iron oxides (Fig. 6i–l).

4.4. Magnetic properties of surficial river sediments

Magnetic property variations in surficial sediments of the major tributaries and main stream of the Yangtze River are shown in Fig. 7. Among the tributaries, the Yalong River, which flows across the E'mei Basalt block in the upper Yangtze basin, has the highest χ_{lf} value (272×10^{-8} m^3/kg) (② Figs. 1B, 7). Notably high χ_{lf} values ($200–230 \times 10^{-8}$ m^3/kg) also occur both at the confluence of the Yalong River and Jinsha River at Yibin (⑤ Figs. 1B, 7) and just below the Three Gorges Valley (⑧ Figs. 1B, 7). The Tuo River tributary of the upper Yangtze has a moderately high χ_{lf} (140×10^{-8} m^3/kg) (⑥ Figs. 1B, 7). In contrast, the tributaries of the mid-lower Yangtze are all characterized by extremely low χ_{lf} values ($5–70 \times 10^{-8}$ m^3/kg) (⑨–⑭ Figs. 1B, 7). SIRM variations in surficial river sediments mirror this χ_{lf} pattern. SIRM maxima reach values $>5000 \times 10^{-5}$ Am^2 kg^{-1} in the Yalong River tributary, which contrasts with other tributaries ($67–1300 \times 10^{-5}$ Am^2 kg^{-1}) (Fig. 7). In the upper tributaries, χ_{ARM}/χ_{lf} and χ_{ARM}/SIRM have low values (Fig. 7). Conversely, higher values of these ratios are evident for tributaries of the mid-lower Yangtze (Fig. 7). S_{-300} values for surficial sediments from the upper tributaries are slightly higher than those of the mid-lower Yangtze (Fig. 7). For the basalt rock

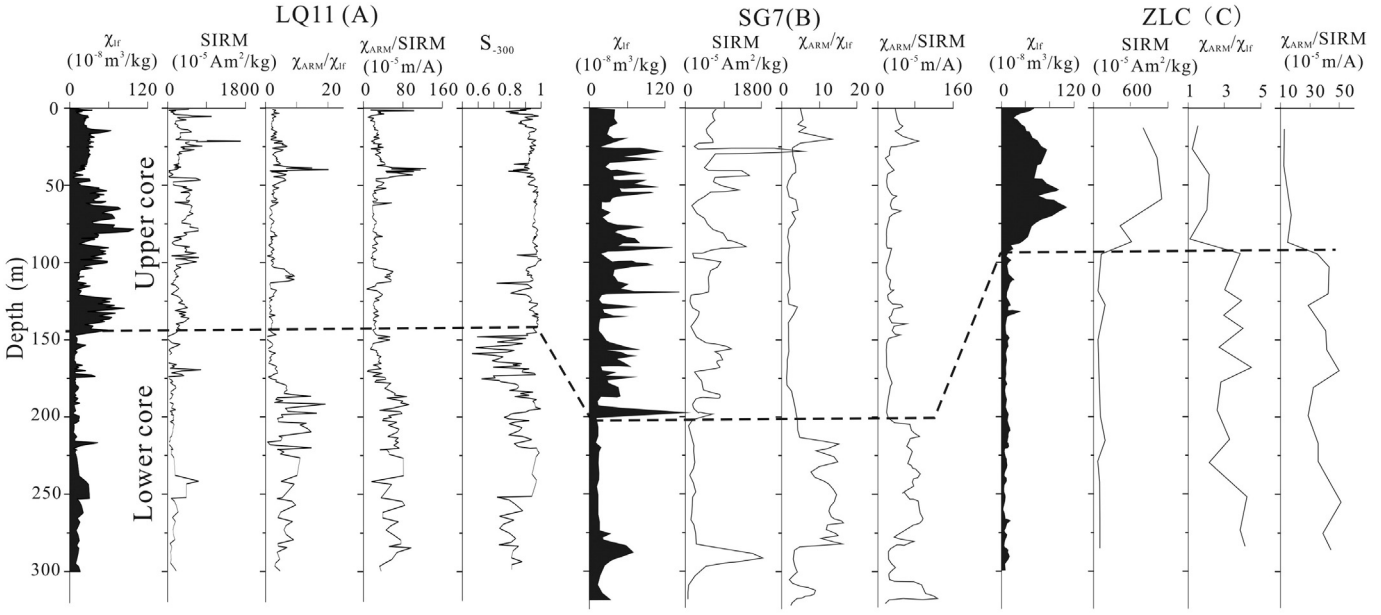

Fig. 5. Comparison of magnetic properties of sediments from cores (A) LQ11, (B) SG7 (Tao, 2007), and (C) ZLC collected from the middle Yangtze (Zhang et al., 2008), and correlation of the magnetic transition at ~1.2–1.0 Ma BP.

sample, χ_{lf} is 1086.7 × 10^{-8} m^3/kg and SIRM can reach 155,776 × 10^{-5} Am^2 kg^{-1}, which is significantly higher than that of all surficial river sediments. χ_{ARM}/χ_{lf} and χ_{ARM}/SIRM are 9.59 and 6.69 × 10^{-5} m/A, respectively, and the S_{-300} value is 0.99 for the basalt (Fig. 7).

A negative correlation with χ_{lf} to χ_{ARM}/SIRM for all samples (both from core sediment, basalt, and surficial sediment) is shown in Fig. 8A; down-core IRM acquisition curves also indicate low coercivities for samples above a depth of 145 m and high coercivities below that depth (Fig. 8B).

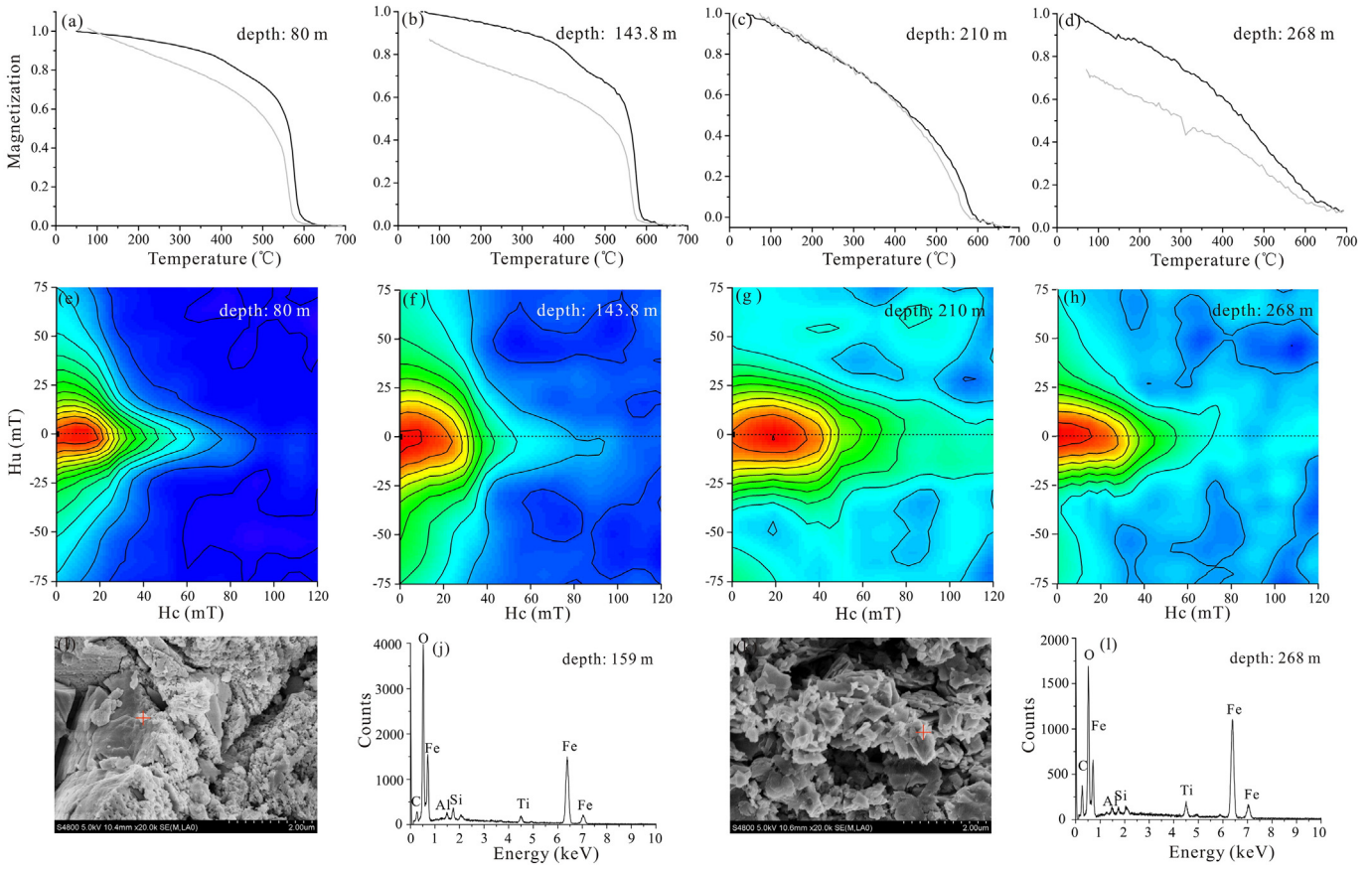

Fig. 6. (a–d) Thermomagnetic curves (black: heating curves; grey: cooling curves), (e-h) First-order reversal curve (FORC) diagrams, (i, k) scanning electron microscope images and (j, l) energy-dispersive spectra for representative samples in core LQ11.

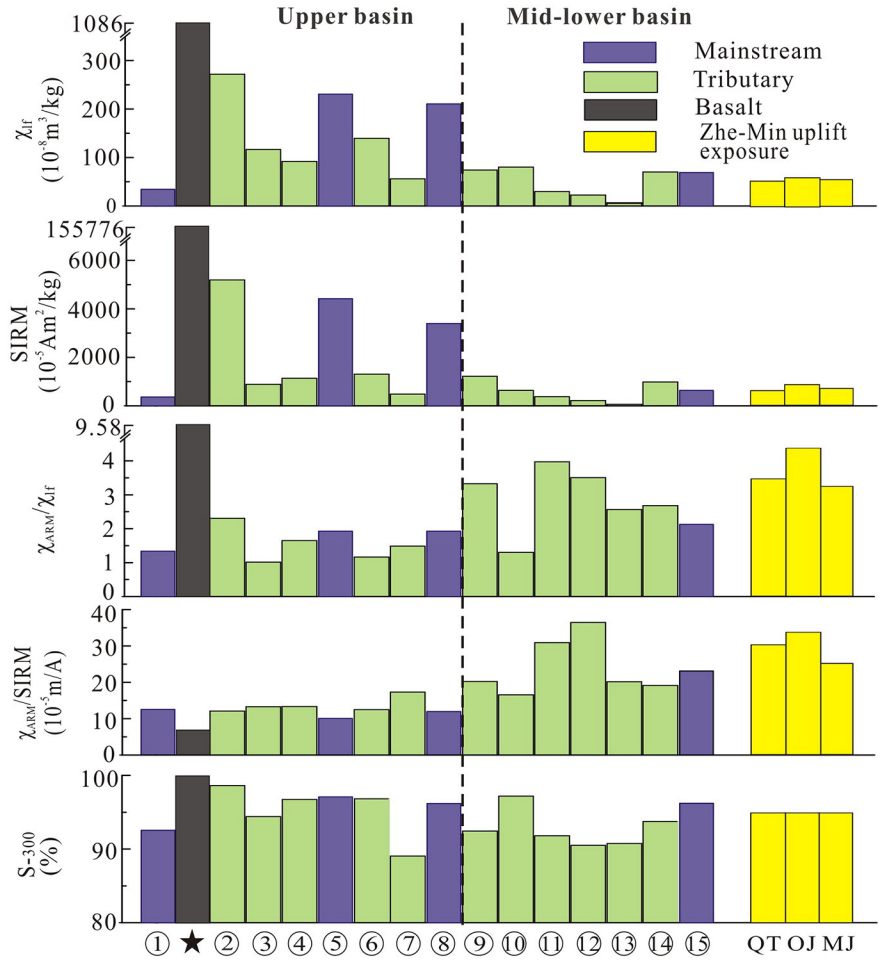

Fig. 7. Distribution of magnetic properties of surficial Yangtze sediments with comparison to the E'mei Basalt and Zhe-Min uplift (①–⑮, ★, and QT, OJ, and MJ see Fig. 1). Samples sourced from tributaries with carbonate and sedimentary rocks have much lower χ_{lf} than those in which basalt is widely distributed in the catchment.

4.5. TOC

TOC contents vary from 0.01 to 3.06% throughout core LQ11, with occasional peaks (Fig. 9). Low TOC values are observed both in Pliocene (0.25–0.33%) and Pleistocene sediment (0.01–1.65%). Occasionally high TOC values occur in the Holocene sediment (0.19–3.06%) (Fig. 9).

4.6. Foraminifera

We identify benthic foraminifera (*Pseudorotalia indopacifica*) at 65 m in core LQ11 (Fig. 2). Large numbers of foraminifera occur almost continuously from 48 to 0 m, except at 42.20–41.30 m (stiff muds of the last Glacial Maximum) (Fig. 2). Most identified foraminifera in this part of the core are shallow marine and estuarine species, e.g. *Ammonia confertitesta*, *Ammonia tepida*, *Cribrononion porisuturalis*, etc.

5. Discussion

5.1. Magnetic property changes in core LQ11: sediment provenance

Magnetic properties of sediments can be affected by changes in particle size distribution (Hatfield and Maher, 2009), post-depositional diagenesis, given a supply of Sulphur, high organic carbon content and at

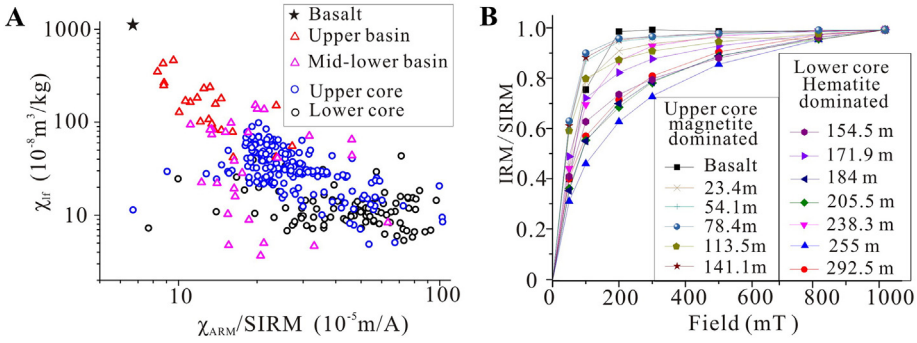

Fig. 8. A) Magnetic susceptibility (χ_{lf}, which is broadly indicative of magnetite concentration) vs. χ_{ARM}/SIRM (higher values indicate finer magnetite grain sizes) for the E'mei Basalt sample, upper and lower core sediments, and surficial river sediments. B) IRM acquisition curves for the E'mei basalt and upper and lower core sediments.

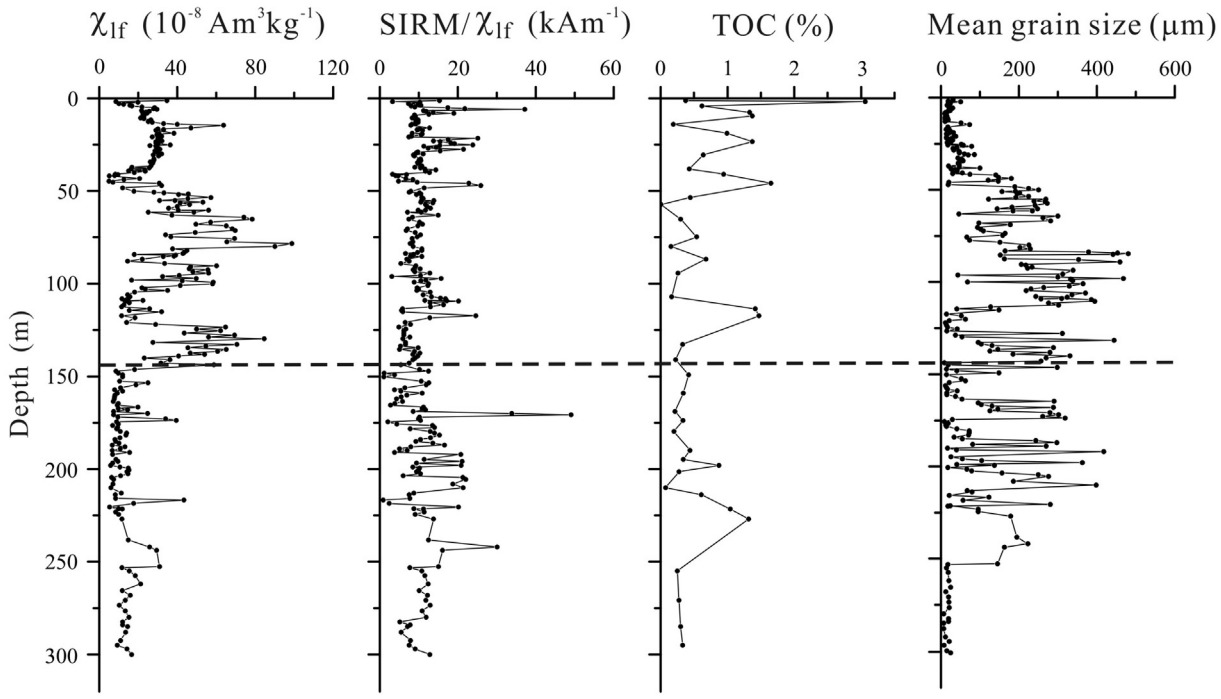

Fig. 9. Relationship of TOC and mean sediment grain size with magnetic properties of core LQ11. Magnetic property changes throughout the upper and lower core sections have no clear relationship to grain size and TOC variations.

least temporarily anoxic conditions (Roberts, 2015), including in situ magnetic mineral formation (Hounslow and Maher, 1999; Roberts, 1995), and sediment provenance (Liu et al., 2012). Particle size varies considerably throughout both the lower and upper core sections, which reflects progressive evolution of sedimentary environments and facies (as below). However, particle size variations appear to have little if any systematic relationship with sediment magnetic properties (Figs. 2, 9). Post-depositional reductive diagenesis generally occurs in various sedimentary facies (Roberts, 2015). It is most likely that high peaks of TOC and SIRM/χ_{lf} in some sediment layers in LQ11 imply greigite formation through diagenetic processes (Fig. 9). However, FORC diagrams, Ms-T curves, and EDS analysis confirm that magnetite is still dominant in these layers (Fig. 6). Diagenesis has not erased the detrital magnetic signal in core LQ11. Therefore, change in sediment provenance is apparently responsible for the observed magnetic property changes throughout both the lower and upper core sections of LQ11.

5.2. Magnetic properties: passive sediment tracer for the eastward connection of the Yangtze River to the sea

The sediment magnetic properties in core LQ11 undergo a shift at a depth of 145 m from low and relatively invariable magnetic mineral concentrations to higher concentrations (Figs. 2, 5A). This step change in ferrimagnetic mineral content above 145 m is evidenced by a distinctive combination of magnetic properties. High χ_{lf}, SIRM, and S_{-300} values, which are indicative of magnetite-like remanence acquisition behavior, are associated with coarse ferrimagnetic grain sizes, as indicated by low χ_{ARM}/χ_{lf} and χ_{ARM}/SIRM values (Fig. 5A). In contrast, the lower portion (below 145 m) of core LQ11 has much lower ferrimagnetic mineral contents that are characterized by finer magnetic mineral grain sizes, and higher hematite concentrations. This major magnetic transition is evident (from χ_{lf} logs) in many other sediment cores in the study area (Fig. 3). Similar contrasts in upper vs lower core magnetic properties were also confirmed in detail in core SG7 from the Yangtze delta (Fig. 5A, B; Tao, 2007).

The distinctive magnetic properties (high χ_{lf}, SIRM, and S_{-300}, and low χ_{ARM}/χ_{lf} and χ_{ARM}/SIRM) of the upper LQ11 sediments can be compared with those of modern river sediments (Fig. 7). A good match is found with strongly magnetic surficial sediments of the upper Yangtze basin where the river has cut through the E'mei Basalt block (Figs. 1B, 5A, 7). Progressive down-river dilution of this magnetically-distinctive upper basin source is evident in space and time because the mid-lower basin tributaries supply relatively weakly magnetic source materials (Figs. 7 and 8A, B). χ_{lf} of both the down-river sediments and upper core sediments declines (lower ferrimagnetic mineral concentrations) as χ_{ARM}/SIRM increases (magnetic grain size becomes finer). In contrast, the low χ_{lf}, SIRM, and S_{-300}, and high χ_{ARM}/χ_{lf} and χ_{ARM}/SIRM values of the lower Pliocene/early Quaternary sediments in core LQ11 appear similar to those of surficial river sediments of the mid-lower Yangtze basin (Figs. 7, 8A, B). Variable mixing of mid-lower basin sources and sediments sourced from the Zhe-Min uplift, along the coast of eastern China, likely contribute to magnetic variability of the lower sediments in core LQ11 (Figs. 1A, 5A, 7, 8A; Cao et al., 2014). The magnetic contrast between the upper and lower core sediments is also evident in their patterns of remanence acquisition. The upper core sediments have soft (easily-magnetized) behavior; while the lower sediments are magnetically harder, which reflects lower magnetite and higher hematite concentrations (Fig. 8B; Thompson and Oldfield, 1986).

The transition in magnetic properties characterized by high χ_{lf}, SIRM, and S_{-300} and low χ_{ARM}/SIRM values in the upper portion of core LQ11 reflects the onset of sediment supply to the Yangtze delta from the extensive (~2.5×10^5 km^2) E'mei Basalt block (Fig. 1B). This distinctive magnetic source outcrops exclusively in the upper basin, i.e. above the Three Gorges Valley. In contrast, the low ferrimagnetic mineral contents in the lower LQ11 sediments reflect the absence of this major magnetic source and, hence, these sediments are interpreted to pre-date opening of the Three Gorges Valley. The paleomagnetic chronology of core LQ11 indicates that this major change in sediment provenance in the proto-Yangtze drainage basin occurred near the base of the Jaramillo subchron at ~1.2–1.0 Ma (Figs. 2, 5A).

High χ_{lf} has been reported previously for the upper portion of a Quaternary sediment core (Zhoulao, ZLC) from immediately below the

Three Gorges Valley, in the mid-Yangtze reach (Figs. 1B, 5C; Zhang et al., 2008). In accord with the LQ11 sequence, this magnetic transition was dated to ~1.2 Ma (Zhang et al., 2008).

Our identification of the upper basin E'mei Basalt block as a key magnetic source is critical. First, our dating of the arrival of this new, strongly-magnetic basaltic source, of exclusively upper-basin origin, confirms that this date marks the opening of the Three Gorges Valley. Second, the synchronous appearance of this new, distinctive sediment source in Yangtze delta sediments indicates that westward extension and connection of the Yangtze River to the East China Sea was complete at this time. These results also accord with recent geochemical studies of detrital magnetite, elemental compositions, and Th-U-Pb ages of monazite (Yang et al., 2006; Gu et al., 2014; Yue et al., 2016).

5.3. Tectonic subsidence recorded by sedimentary facies: geological forcing of the proto-Yangtze connection to the sea

Independent of our magnetic interpretation, the temporal sequence of sedimentary facies and environmental changes recorded by core LQ11, and many other cores in the study area, provides a record of tectono-geomorphologic evolution of the Yangtze catchment. The unconformable basal contact with igneous and sedimentary Paleozoic-Mesozoic bedrock indicates the existence of local uplands in eastern China (Wang, 1985a, 1985b), and an erosional and/or weathering hiatus prior to the Late Pliocene onset of terrestrial deposition in the present-day delta. Basal Late Pliocene sediments in core LQ11 (300.5–252 m) are reddish mudstones, which indicate lacustrine deposition under a relatively warm and/or arid climate. Thick Early Pleistocene sedimentary cycles (252–112 m) comprise basal gravelly sands topped by silty clay, which reflects alluvial-fan deposition (Figs. 2, S1). Thinning, fining and the appearance of cross-stratification in Middle Pleistocene sediments (112–67.6 m) indicate a gradual change from alluvial to fluvial deposition (Figs. 2, S1). Cyclic Late Pleistocene sediments (67.6–41.3 m), with basal coarse sands to fine sand and silt on top, are associated with the episodic appearance of marine foraminifera, from 65 m upward (Figs. 2, S1). Our previous study of a neighboring sediment core, CH1, ~20 km north of LQ11, indicates the continuous presence of foraminifera from ~85 m upward (Chen et al., 1997). These data indicate Late Pleistocene marine transgression along the coast near the Yangtze River mouth (Fig. 2; Qiu and Li, 2007). The study area was briefly exposed subaerially, as marked by the stiff muds of the LGM (42.20–41.30 m) when global sea level fell (Figs. 2, S1; Chen et al., 2008). The Yangtze delta of the study area formed only in the Holocene.

Sedimentary facies changes, from upland alluvial/fluvial environments to a coastal/deltaic setting, are consistent with continuous tectonic subsidence, which affected much of the east coast of China since the early Quaternary (Chen and Stanley, 1995). Subsidence of the study area coincided with submergence of the Zhe-Min uplift (Fig. 1A) on the East China Sea shelf, which was initiated in the early Quaternary (Yi et al., 2014). This subsidence was controlled by collision between the Eurasian and the Pacific plates, in contrast with Tibetan Plateau uplift in western China, which was driven by collision between the Indian and Eurasian plates. This so-called Cenozoic Topographic Reversal (Fig. 1A, B; Wang, 1990) provided the continental-scale forcing for evolution of local river basins in the lower Yangtze to be gradually connected westward to the upper Yangtze basin.

5.4. The northern Yangtze delta coast: a possible earlier site of proto-Yangtze connection to the sea

Of note, the northern Yangtze delta plain was suggested to be the early route for proto-Yangtze flow into the sea (Fig. 1C; Chen and Stanley, 1995). Geological surveys indicate that the northern Yangtze was a semi-closed (seaward open) basin during the Neogene time, during which thick (>1000 m) terrestrial consolidated sediments were deposited (Chen and Stanley, 1995). Therefore, the proto-Yangtze connection to the sea along the northern coast presumably occurred earlier than movement to the present position of the river mouth area, which could be inferred from limited magnetic work on the northern delta region (Shu et al., 2008). Future magnetic analysis of Cenozoic sediments magnetic analyses in the northern delta region will offer a potential answer to this unresolved question.

6. Conclusions

Mineral magnetic and paleomagnetic properties of the Plio-Quaternary sediment sequence from the present-day Yangtze delta provide key information about the source and timing of a fundamental shift in sediment provenance and river basin evolution. Late Pliocene/Early Quaternary sediments are weakly magnetic, and were sourced from Paleozoic-Mesozoic sedimentary rocks and Quaternary sediments in eastern China. The switch to more abundant and coarser magnetic minerals at ~1.2–1.0 Ma reflects westward extension of the Yangtze, via the opening of the Three Gorges Valley, and the onset of sediment supply from a new, upper-basin source, with a strongly magnetic signal from the E'mei basalt. Magnetic analysis of modern surficial river sediments confirms similarly strong magnetic properties between the upper LQ11 sediment and those of the upper Yangtze basin sediments. Our chronostratigraphic evidence indicates that both the new sediment source and the connection to the East China Sea were initiated no later than ~1.2–1.0 Ma.

Supplementary data to this article can be found online at https://doi.org/10.1016/j.geomorph.2017.11.023.

Acknowledgements

This project was supported financially by the National Natural Science Foundation of China (Grant No. 41620104004 and 41771226) and Chinese Postdoctoral Science Foundation (Grant No. 2017M611611). We are grateful to Andrew P. Roberts and an anonymous reviewer for their constructive comments.

References

Bloemendal, J., King, J.W., Hall, F.R., Doh, S.J., 1992. Rock magnetism of Late Neogene and Pleistocene deep-sea sediments: relationship to sediment source, diagenetic processes, and sediment lithology. J. Geophys. Res. 97 (B4), 4361–4375.

Brookfield, M.E., 1998. The evolution of the great river systems of southern Asia during the Cenozoic India-Asia collision: rivers draining southwards. Geomorphology 22 (3), 285–312.

Cande, S.C., Kent, D.V., 1995. Revised calibration of the geomagnetic polarity timescale for the Late Cretaceous and Cenozoic. J. Geophys. Res. 100 (B4), 6093–6095.

Cao, W.H., Chen, J., Ma, J.Q., 2014. Magnetic minerals as tracers for the mainland coastal rivers and west Taiwan rivers. Quatern. Sci. 36 (1), 227–236 (in Chinese with English abstract).

Changjiang Water Resources Commission, 1999. Atlas of Changjiang River Basin. Geological Publishing House, Beijing, pp. 32–33 (in Chinese).

Chen, Z.Y., Stanley, D.J., 1995. Quaternary subsidence and river channel migration in the Yangtze Delta Plain, Eastern China. J. Coastal. Res. 11 (3), 927–945.

Chen, Z.Y., Chen, Z.L., Zhang, W.G., 1997. Quaternary stratigraphy and trace-element indices of the Yangtze delta, eastern China, with special reference to marine transgressions. Quat. Res. 47 (2), 181–191.

Chen, Q.Q., Li, C.X., Li, P., Liu, B.Z., Sun, H.P., 2008. Late Quaternary palaeosols in the Yangtze Delta, China, and their palaeoenvironmental implications. Geomorphology 100 (3), 465–483.

Chen, J., Wang, Z.H., Wei, T.Y., Zhao, B.C., Chen, Z.Y., 2014. Clay minerals in the Pliocene-Quaternary sediments of the southern Yangtze coast, China: sediment sources and palaeoclimate implications. J. Palaeogeogr. 3 (3), 297–308.

Clark, M.K., Royden, L.H., Whipple, K.X., Burchfiel, B.C., Zhang, X., Tang, W., Wang, E., Chen, L., 2004. Surface uplift, tectonics, and erosion of eastern Tibet from large-scale drainage patterns. Tectonics 23 (1), TC1006. https://doi.org/10.1029/2002TC001402.

Clift, P.D., Blusztajn, J., Nguyen, A.D., 2006. Large-scale drainage capture and surface uplift in eastern Tibet–SW China before 24 Ma inferred from sediments of the Hanoi Basin, Vietnam. Geophys. Res. Lett. 33 (19). https://doi.org/10.1029/2006GL027772 (L19403).

Fan, D.D., Li, C.X., Yokoyama, K., Zhou, B.C., Li, B.H., Wang, Q., Yang, S.Y., Deng, B., Wu, G.X., 2005. Monazite age spectra in the Late Cenozoic strata of the Changjiang delta and its implication on the Changjiang run-through time. Sci. China Ser. D. 48 (10), 1718–1727.

Gu, J.W., Chen, J., Sun, Q.L., Wang, Z.H., Wei, Z.X., Chen, Z.Y., 2014. China's Yangtze delta: geochemical fingerprints reflecting river connection to the sea. Geomorphology 227, 166–173.
Hatfield, R.G., Maher, B.A., 2009. Fingerprinting upland sediment sources: particle size-specific magnetic linkages between soils, lake- and suspended sediments. Earth Surf. Proc. Land. 34 (10), 1359–1373.
Heslop, D., Roberts, A.P., 2012. Estimation of significance levels and confidence intervals for first-order reversal curve distributions. Geochem. Geophys. Geosyst. 13 (Q12Z40). https://doi.org/10.1029/2011jb008859.
Hoorn, C., 1994. An environmental reconstruction of the paleo Amazon River system (Middle-Late Miocene, NW Amazonia). Palaeogeogr. Palaeoclimatol. Palaeocol. 112 (3–4), 187–238.
Hounslow, M.W., Maher, B.A., 1999. Source of the climate signal recorded by magnetic susceptibility variations in Indian Ocean sediments. J. Geophys. Res. 104 (B3), 5047–5061.
Kirschvink, J.L., 1980. The least-squares line and plane and the analysis of palaeomagnetic data. Geophys. J. Int. 62 (3), 699–718.
Li, J.J., Xie, S.Y., Kuang, M.S., 2001. Geomorphic evolution of the Yangtze Gorges and the time of their formation. Geomorphology 41 (2), 125–135.
Liu, Q.S., Roberts, A.P., Larrasoaña, J.C., Banerjee, S.K., Guyodo, Y., Tauxe, L., Oldfield, F., 2012. Environmental magnetism: principles and applications. Rev. Geophys. 50 (4). https://doi.org/10.1029/2012RG000393.
Malusà, M.G., Resentini, A., Garzanti, E., 2016. Hydraulic sorting and mineral fertility bias in detrital geochronology. Gondwana Res. 31, 1–19.
Pike, R.C., Roberts, A.P., Verosub, K.B., 1999. Characterizing interactions in fine magnetic particle systems using first order reversal curves. J. Appl. Phys. 105 (B12), 28461–28475.
Qiu, J.B., Li, X., 2007. Quaternary Stratigraphy and Sedimentary Environment of Shanghai. Shanghai Science and Technology Press, Shanghai, pp. 112–116 (in Chinese).
Richardson, N.J., Densmore, A.L., Seward, D., Wipf, M., Yong, L., 2010. Did incision of the Three Gorges begin in the Eocene? Geology 38 (6), 551–554.
Roberts, A.P., 1995. Magnetic properties of sedimentary greigite (Fe_3S_4). Earth Planet. Sci. Lett. 134 (3–4), 227–236.
Roberts, A.P., 2015. Magnetic mineral diagenesis. Earth-Sci. Rev. 151, 1–47.
Roberts, A.P., Pike, C.R., Verosub, K.L., 2000. First-order reversal curve diagrams: a new tool for characterizing the magnetic properties of natural samples. J. Geophys. Res. 105 (B12), 28461–28475.
Roberts, A.P., Heslop, D., Zhao, X., Pike, C.R., 2014. Understanding fine magnetic particle systems through use of first-order reversal curve diagrams. Rev. Geophys. 52: 557–602. https://doi.org/10.1002/2014RG000462.
Said, R., 1981. The Geological Evolution of the River Nile. Springer, New York, pp. 1–11.
Shu, Q., Zhang, M., Zhao, Z., Chen, Y., Li, J., 2008. Sedimentary record from the XH-1 core in north Jiangsu basin and its implication on the Yangtze River run-through time. J. Stratigr. 32 (3), 308–314 (in Chinese with English abstract).
Tao, S.K., 2007. Magnetic Properties of late Cenozoic Sediments in the Yangtze River Delta and Implications for Their Sedimentary Environment, Provenance and Paleoclimate. MSc thesis. East China Normal Univ., Shanghai, China (in Chinese with English abstract).
Thompson, R., Oldfield, F., 1986. Environmental Magnetism. Allen and Unwin, London, pp. 39–48.
Wang, H.Z., 1985a. Atlas of the Palaeogeograpy of China. Cartographic Publishing House, Beijing, pp. 125–138 (in Chinese).
Wang, P.X., 1985b. Marine Micropaleontology of China. China Ocean Press, Beijing, pp. 1–370.
Wang, P.X., 1990. Neogene stratigraphy and paleoenvironments of China. Palaeogeogr. Palaeoclimatol. Palaeocol. 77, 315–334.
Wang, P.X., Clemens, S., Beaufort, L., Braconnot, P., Ganssen, G., Jian, Z.M., Kershaw, P., Sarnthein, M., 2005. Evolution and variability of the Asian monsoon system: state of the art and outstanding issues. Quat. Sci. Rev. 24 (5), 595–629.
Wang, Z.H., Zhang, D., Li, X., Tao, S.K., Xie, Y., 2008. Magnetic properties and relevant minerals of late Cenozoic sediments in the Yangtze River delta and their implications. Geol. China 35 (4), 670–682 (in Chinese with English abstract).
Xiang, F., Zhu, L.D., Wang, C.S., Zhao, X.X., Chen, H.D., Yang, W.G., 2007. Quaternary sediment in the Yichang Area: implications for the formation of the Three Gorges of the Yangtze River. Geomorphology 85 (3–4), 249–258.
Yang, S.Y., Li, C.X., Yokoyama, K., 2006. Elemental compositions and monazite age patterns of core sediments in the Changjiang Delta: implications for sediment provenance and development history of the Changjiang River. Earth Planet. Sci. Lett. 245 (3), 762–776.
Yi, L., Ye, X.Y., Chen, J.B., Li, Y., Long, H., Wang, X.L., Du, J.H., Zhao, S.L., Deng, C.L., 2014. Magnetostratigraphy and luminescence dating on a sedimentary sequence from northern East China Sea: constraints on evolutionary history of eastern marginal seas of China since the Early Pleistocene. Quat. Int. 349, 316–326.
Yue, W., Liu, J.T., Zhang, D., Wang, Z.H., Zhao, B.C., Chen, Z.Y., Chen, J., 2016. Magnetite with anomalously high Cr_2O_3 as a fingerprint to trace upper Yangtze sediments to the sea. Geomorphology 268, 4–20.
Zhang, Y.F., Li, C.A., Wang, Q.L., Chen, L., Ma, Y.F., Kang, C.G., 2008. Magnetism parameters characteristics of drilling deposits in Jianghan Plain and indication for forming of the Yangtze River Three Gorges. Chin. Sci. Bull. 53 (4), 584–590.
Zheng, S., Fu, Z., 2000. Fauna Sinica. Phylum Granuloreticulosa, Class Foraminiferea, Agglutinated Foraminifera. Science Press, Beijing, pp. 1–788.
Zheng, H.B., Clift, P.D., Wang, P., Tada, R., Jia, J.T., He, M.Y., Jourdan, F., 2013. Pre-Miocene birth of the Yangtze River. Proc. Natl. Acad. Sci. U. S. A. 110, 7556–7561.
Zijderveld, J.D.A., 1967. AC demagnetization of rocks: analysis of results. In: Collinson, D.W., Creer, K.M., Runcorn, S.K. (Eds.), Methods in Paleomagnetism. Elsevier, New York, pp. 254–286.